Available online at www.sciencedirect.com
SCIENCE DIRECT
Journal of Catalysis 236 (2005) 139–152
JOURNAL OF CATALYSIS
www.elsevier.com/locate/jcat

Characterization of alumina-, silica-, and titania-supported cobalt Fischer–Tropsch catalysts

Sølvi Storsæter [a], Bård Tøtdal [b], John C. Walmsley [c], Bjørn Steinar Tanem [c], Anders Holmen [a,*]

[a] *Department of Chemical Engineering, Norwegian University of Science and Technology (NTNU), N-7491 Trondheim, Norway*
[b] *Department of Physics, Norwegian University of Science and Technology (NTNU), N-7491 Trondheim, Norway*
[c] *SINTEF Materials and Chemistry, Synthesis and Properties, N-7491 Trondheim, Norway*

Received 27 July 2005; revised 12 September 2005; accepted 16 September 2005

Available online 20 October 2005

Abstract

Co and CoRe supported on γ-Al_2O_3, SiO_2, and TiO_2 were prepared by incipient wetness impregnation. The influence of the different supports on the shape, appearance, and size of cobalt particles, as well as on reducibility, was studied by different techniques, including X-ray diffraction, scanning transmission electron microscopy, H_2 chemisorption, N_2 adsorption measurements, temperature-programmed reduction, and O_2 titration. Co was found to exist as Co_3O_4 on the catalysts in their calcined state. Co_3O_4 particle size, Co^0 particle size, and reducibility increased with increasing average pore diameter of the support. On both γ-alumina and silica, Co_3O_4 appeared in clusters, with larger clusters for the silica support, which has a larger average pore diameter. However, on TiO_2, Co_3O_4 existed as single crystals, as it also did on α-alumina with large average pore diameter. Thus the size of Co_3O_4 agglomerates probably increases with increasing pore size up to a certain pore size, beyond which no agglomeration will occur. Rhenium was evenly distributed over the substrate surface, but higher concentrations of rhenium were found at the cobalt-containing positions. Activity and selectivity data obtained previously are discussed in terms of cluster size, particle size, and mass transport limitations.

Keywords: Fischer–Tropsch synthesis; Cobalt; Rhenium; Alumina; Silica; Titania; TEM; Pore diameter; XRD; TPR; H_2-chemisorption; Pulse oxidation; Selectivity

1. Introduction

Supported cobalt has been widely studied as a Fischer–Tropsch (FT) catalyst for the conversion of synthesis gas derived from natural gas, due to its high activity, high selectivity to long-chain paraffins, and low water–gas shift activity. The support seems to be an important factor in the properties of the catalysts. Cobalt in its reduced state, not cobalt precursors, is the active component in the CO/H_2 reaction. Two major factors determine catalyst activity ($g_{prod}/(g_{cat}\,h)$), namely the degree of reduction of the metal precursor and the shape and size of the metal particles formed, which control the number of active sites available (dispersion). If a change in dispersion does not lead to a change in turnover frequency, then, by definition, the reaction is structure-insensitive.

The type and structure of the support influence the dispersion, particle size and reducibility, and thereby the activity for Co-supported catalysts [1–19]. C_{5+} selectivity is also affected by the type of support and the promoter [1,10,12,16–18,20,21]. The acidity of alumina supports [22,23] and modification of silica supports by the addition of zirconia [24,25] are other factors that affect FT activity through changes in reducibility and dispersion. However, zirconia increases the FT activity for an alumina-supported Co catalyst with no corresponding increase in reducibility or dispersion [26,27]. Furthermore, in most cases different promoters also affect dispersion and reducibility [2,7,28–39]. Besides the support and promoter, several other preparation variables, including cobalt precursor and solvent [6,40–46], cobalt loading [3,4,7,44,47–49], preparation method [3,42,50,51], and pretreatments (e.g., the conditions during drying

* Corresponding author. Fax: +47 73595047.
E-mail address: holmen@chemeng.ntnu.no (A. Holmen).

0021-9517/$ – see front matter
doi:10.1016/j.jcat.2005.09.021

Table 1
Hydrocarbon formation rate and selectivity to CH_4 and C_{5+} at 40–45% CO conversion. $H_2/CO = 2.1$, $P_{Tot} = 20$ bar and $T = 210\,^{\circ}C$ [17]

Catalyst	GHSV ($ml/(g_{cat}\,h)$)	CO conversion (%)	Hydrocarbon formation rate ($g_{HC}/(g_{cat}\,h)$)	Selectivity (%)[a]		Structural parameter $\chi \times 10^{16}$ (m^{-1})[b]
				CH_4	C_{5+}	
$Co/\gamma\text{-}Al_2O_3$	2982	42.6	0.25	9.7	80.2	33
$CoRe/\gamma\text{-}Al_2O_3$	5960	42.8	0.42	8.8	80.8	52
Co/SiO_2	3060	40.4	0.24	9.1	81.7	12
$CoRe/SiO_2$	4166	40.3	0.33	8.7	83.4	12
Co/TiO_2	1885	39.8	0.14	9.8	82.3	7
$CoRe/TiO_2$	3595	42.6	0.30	8.9	84.8	7

[a] The uncertainty ($\pm 2\sigma$) is estimated to be ±0.4% based on the standard deviation of repeated measurements.
[b] Structural parameter calculated according to equation (2) [21].

and calcination [6,52–55] and reduction [56–61]), affect the reducibility and dispersion of the catalysts.

The most usual methods for cobalt particle size and dispersion determinations are H_2 chemisorption, X-ray diffraction (XRD), X-ray photoelectron spectroscopy, and extended X-ray absorption fine structure spectroscopy (EXAFS). However, these methods say nothing about the shape and morphology of the particles or how they exist in relation to each other. Transmission electron microscopy (TEM) is a valuable method for obtaining this information. Co_3O_4 has been found as clusters on silica supports [16,19,25], but conflicting results on the dependence of the size of these clusters on pore diameter have been reported. Different studies have found that the cluster size increases [16] and decreases [19] with increasing pore diameter of the silica support.

TEM is a widely used technique for collecting information about small metal particles. However, few studies of cobalt-supported catalysts involve TEM investigations. Voß et al. [13] characterized Co catalysts supported on alumina, silica, and titania by several techniques, including electron microscopy. The catalysts were studied in the calcined state. The effect of reduction temperature on the cobalt particles supported on high- and low-surface area silica was studied by Jabłoński et al. [59] using TEM. The catalysts were reduced ex situ and passivated in air before performing the TEM. Some preliminary results from our work using scanning TEM (STEM) for studying CoRe catalysts supported on $\gamma\text{-}Al_2O_3$, SiO_2, and TiO_2 have been presented previously [62].

It has been shown that the reaction rate to long-chain hydrocarbons and the C_{5+} selectivity over supported Co catalysts depend on the type and structure of the support [17,18]. The greatest long-chain hydrocarbon selectivity is observed for a promoted TiO_2-supported cobalt catalyst, and the highest reaction rate is observed for a promoted high-surface area $\gamma\text{-}Al_2O_3$-supported cobalt catalyst. The effect of water on FT activity and selectivity for a series of unpromoted and Re-promoted Co catalysts supported on high-surface area alumina, high-surface area silica, and low-surface area titania has been recently reported [17]. The results obtained at 40–45% conversion are given in Table 1. Activity and selectivity data obtained shortly after 20% water addition are presented in Table 2. It was found that water increases the selectivity to long-chain hydrocarbons for all supports and that it initially increases the activity for silica- and titania- supported catalysts, whereas deactivation was observed for the γ-alumina-supported catalysts. For the silica-supported catalysts, in addition to increased activity, the rate of deactivation was greater than before water addition. For the titania-supported catalysts, very little deactivation was observed. The effect of water has also been studied by others, and similar results showing that water has a significant effect on FT synthesis have been obtained [2,30,63–70]. The reason why water affects the reaction rate to hydrocarbons differently with dissimilar supports remains incompletely understood.

Table 2
Conversion, activity and selectivity shortly after addition of about 20% water at 40–45% conversion. $H_2/CO = 2.1$, $P_{Tot} = 20$ bar, $T = 210\,^{\circ}C$

Catalyst	CO conversion (%)	Hydrocarbon formation rate ($g_{HC}/(g_{cat}\,h)$)	Selectivity (%)[a]	
			CH_4	C_{5+}
$Co/\gamma\text{-}Al_2O_3$	39.5	0.23	6.7	83.0
$CoRe/\gamma\text{-}Al_2O_3$	35.1	0.34	6.5	83.8
Co/SiO_2	46.0	0.28	5.4	87.5
$CoRe/SiO_2$	46.4	0.38	5.1	88.6
Co/TiO_2	47.8	0.18	5.2	90.1
$CoRe/TiO_2$	53.1	0.37	4.7	91.4

[a] The uncertainty ($\pm 2\sigma$) is estimated to be ±0.4% based on the standard deviation of repeated measurements.

The main reason for using TEM to study cobalt-supported catalysts is to investigate the shape, size, and orientation of the Co particles on different supports, and then determine how this may contribute to the different behavior observed during the FT synthesis. We also discuss the performance of the different catalysts in terms of mass transfer limitations and the structural parameter χ introduced by Iglesia et al. [21].

2. Experimental

2.1. Catalyst preparation

Catalysts containing 12 wt% Co and 12 wt% Co/0.5 wt% Re were prepared by incipient wetness coimpregnation of different supports with aqueous solutions of $Co(NO_3)_2{\cdot}6H_2O$ and $HReO_4$. The following supports were included in the study: $\gamma\text{-}Al_2O_3$ (Puralox SCCa-5/200 from Condea, treated with air at 500 °C for 10 h), SiO_2 (PQ corp. CS-2133, treated with air at 500 °C for 10 h) and TiO_2 (Degussa P25, treated with air at 700 °C for 10 h). The catalysts were dried in air at 120 °C for 3 h before calcination in air at 300 °C for 16 h. The catalysts

were sieved to 53–90 μm. For use during the STEM studies, a α-Al_2O_3 sample containing 20% Co/0.5% Re was prepared in the same way as above.

2.2. H_2 chemisorption

H_2 adsorption isotherms were measured at 40 °C in a standard volumetric glass apparatus (Micromeritics ASAP 2010) capable of obtaining a vacuum of 10^{-5} Torr or better. The reactor was loaded with 0.2–0.5 g of catalyst. Before measurements, the catalysts were reduced in flowing hydrogen with temperature programming from ambient to 350 °C at a rate of 1 °C/min. This temperature was maintained for 10 h. After reduction, the samples were evacuated for 0.5 h at 330 °C before cooling to 40 °C, and the adsorption isotherm was measured between 10 and 510 mmHg. The amount of hydrogen chemisorbed was determined by extrapolating the linear part of the isotherm to zero pressure. It is assumed that Re does not contribute to the amount of hydrogen chemisorbed when calculating the dispersion [29] and that the adsorption stoichiometriy is H:Co = 1.

Assuming spherical particles, the Co^0 particle size (d_p) is related to the dispersion (D) through the following formula [71]:

$$d_p = \frac{96}{D}. \quad (1)$$

2.3. BET surface area and pore size measurements

Surface area measurements were performed in a Carlo Erba Multisampler 1900 apparatus by N_2 adsorption. The samples (particle size 53–90 μm) were evacuated and dried at 150 °C before analysis. The surface area was calculated as the Brunauer–Emmett–Teller (BET) surface area.

Pore diameter, pore size distribution, and pore volume were determined by N_2 adsorption in a Micromeritics Tristar 3000 instrument for the γ-Al_2O_3- and SiO_2-supported catalysts and by Hg intrusion using a Carlo Erba Porosimeter 2000 for the TiO_2-supported catalysts. The samples were degassed at 200 °C overnight before measurement. Total pore volume and pore size distribution were calculated form the nitrogen desorption curve using the Barrett–Joyner–Halenda (BJH) method [72].

2.4. X-Ray diffraction

XRD studies were performed in a Philips PW 1710 spectrometer at ambient temperature using monochromatic Cu-K_α radiation. The measurements were done on crushed calcined catalysts and average Co_3O_4 particle sizes were calculated from the most intense Co_3O_4 line ($2\theta = 36.9°$), using the Scherrer formula [73].

2.5. Temperature-programmed reduction

Temperature-programmed reduction (TPR) studies were performed in a U-shaped tubular quartz reactor heated by an electrical furnace, for both calcined and reduced catalysts. For the TPR studies of calcined catalysts, the reactor was loaded with 0.2 g of catalyst and heated at a rate of 10 °C/min to 930 °C in a gas consisting of 7% H_2 in Ar. The gas flow rate was 30 ml/min. For the TPR experiments for reduced catalysts, 0.5 g of catalyst was loaded into the reactor. The catalyst was reduced in situ in a flow of hydrogen (30 ml/min) with temperature programming from ambient to 350 °C at a rate of 1 °C/min. This temperature was maintained for 16 h before reducing the temperature to 25 °C. The catalyst was flushed with Ar for 1 h and then heated at a rate of 10 °C/min to 930 °C in a gas consisting of 7% H_2 in Ar (30 ml/min). H_2 consumption was measured by analyzing the effluent gas using a thermal conductivity detector, and calibration was done by reduction of Ag_2O powder.

2.6. Pulse oxidation

The extent of reduction was determined by pulse oxidation with O_2 of reduced samples at 400 °C in the same apparatus as used for the TPR experiments. After reduction at 350 °C for 10 h (heating rate 1 °C/min), the sample was heated to 400 °C in He and held for 1 h to desorb any chemisorbed H_2. Calibrated pulses of O_2 were then added into the continuous He flow until no further consumption of O_2 was detected by the thermal conductivity detector located downstream of the reactor. The amount of O_2 consumed was calculated from the known pulse volume, temperature, pressure, and the number of pulses reacting with the catalyst. The extent of reduction was calculated assuming stoichiometric reoxidation of Co^0 to Co_3O_4.

2.7. Electron microscopy

Sample preparation was done by two different techniques and examined using two different microscopes. The first preparation method (denoted by PM1) was used for the γ-Al_2O_3-, SiO_2-, and TiO_2-supported catalysts. Calcined catalysts were crushed before they were sprinkled on a “holey carbon” film supported on Ti grids. These samples were analyzed in a dedicated scanning transmission electron microscope (VG HB-603) using a Si(Li) detector connected to an INCA analytical system (Oxford Instruments). The beam voltage was 300 kV. Energy dispersive spectrometry (EDS) was used to confirm the presence and location of the different species in the samples. The chemical phase of cobalt on the catalyst was obtained by comparing the diffraction pattern of a reference material with diffraction patterns from the samples. STEM images were recorded using an annular dark-field detector, giving a signal that is sensitive to the local atomic number in the sample.

Thinner samples with a more even surface were obtained by the second method, PM2, using ultramicrotomy as follows. A small amount of the uncrushed catalyst particles was embedded in a two-component epoxy resin and stored overnight at 40 °C. Thin slices of the samples were obtained by cutting the embedded catalyst with a diamond knife using a model ultramicrotome. The resulting sample slices were collected on a Cu mesh grid and analyzed in a Philips CM30 transmission electron microscope at 200 kV.

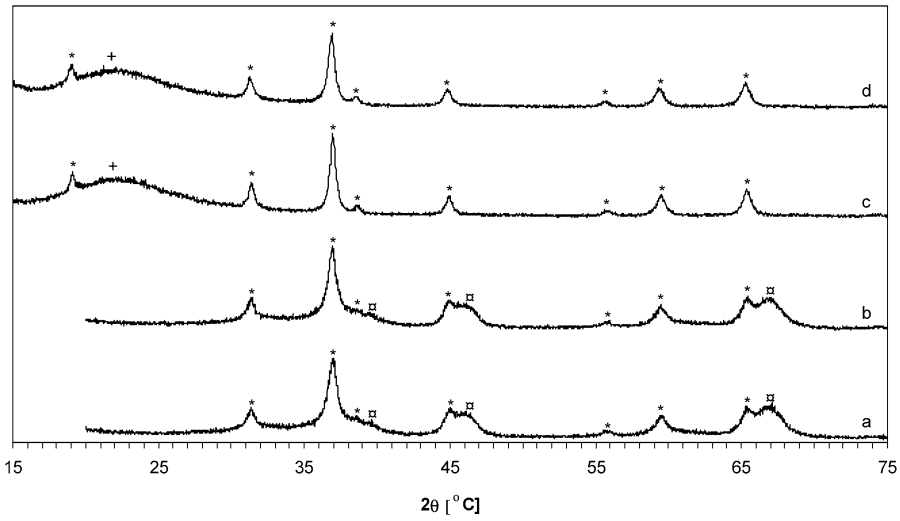

Fig. 1. X-Ray diffraction pattern for (a) Co/γ-Al_2O_3, (b) CoRe/γ-Al_2O_3, (c) Co/SiO_2, and (d) CoRe/SiO_2. Phases denoted are (∗) Co_3O_4, (¤) γ-Al_2O_3 and (+) SiO_2.

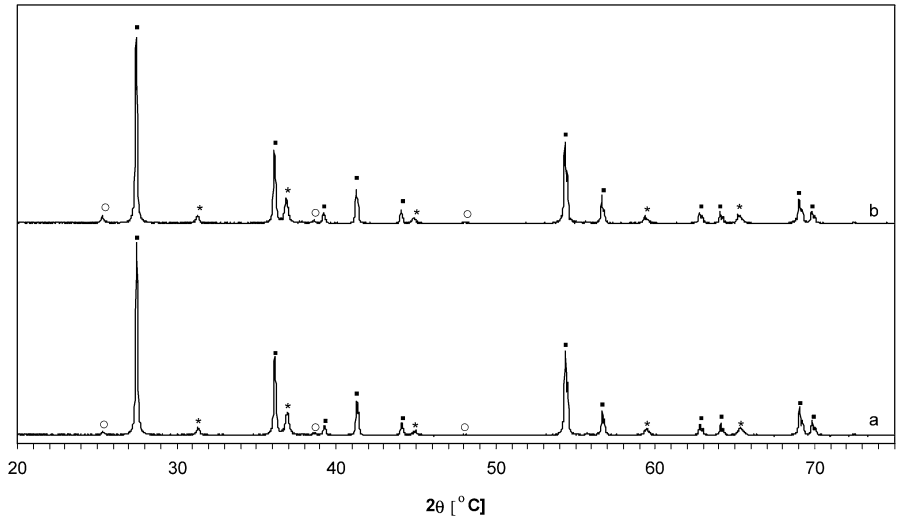

Fig. 2. X-Ray diffraction pattern for (a) Co/TiO_2 and (b) CoRe/TiO_2. Phases denoted are (∗) Co_3O_4, (○) anatase TiO_2 and (■) rutile TiO_2.

3. Results and discussion

3.1. X-Ray diffraction, H_2 chemisorption, and pore measurements

Fig. 1 shows the XRD patterns of Co and CoRe supported on γ-Al_2O_3 (a and b) and SiO_2 (c and d). The location of the peaks confirms that Co_3O_4 was the only crystalline phase of Co present. Except for Co_3O_4, only peaks for amorphous SiO_2 and γ-Al_2O_3 were detected. No Re was observed in the XRD patterns. Fig. 2 shows the XRD patterns for the Co/TiO_2- and CoRe/TiO_2-supported catalysts. Due to the high-temperature calcination (700 °C) of the TiO_2 support before impregnation, the support was present mostly in its rutile phase. In this case, Co was also detected only as crystalline Co_3O_4.

As stated earlier, the width at half maximum of the most intense Co_3O_4 peak, $2\theta = 36.9°$, was used to calculate the Co_3O_4 particle size. Narrow Co_3O_4 peaks indicate large particles, whereas broad peaks correspond to small particles. For average particle size calculation from XRD, calculating the size in different directions found that a spherical shape was a good approximation for the Co_3O_4 particles. The average Co_3O_4 particle size calculated for all catalysts from the Scherrer equation, together with the average Co^0 particle sizes obtained from H_2 chemisorption measurements, are given in Table 3. The average Co_3O_4 particle size, as determined by XRD, was smallest for the γ-Al_2O_3-supported catalysts and slightly larger for the SiO_2-supported catalysts. The largest Co_3O_4 particles were observed on the TiO_2-supported catalyst. Although Re had only an insignificant influence on the average Co_3O_4 particle size for the γ-Al_2O_3- and SiO_2-supported catalysts, Re increased the average Co_3O_4 particle size for the TiO_2-supported catalysts.

The same trend between support and average Co^0 particle size was found from the H_2 chemisorption results (Table 3). However, in this case Re influenced the average Co^0 particle size for the SiO_2- and TiO_2-supported catalysts only slightly, whereas for the γ-Al_2O_3-supported catalysts, promoting with

Table 3
Co^0 particle size and dispersion from H_2 chemisorption, and Co_3O_4 particle size from XRD

Catalyst	Dispersion (H_2-ads.) (%)[a]	Co^0 particle size (H_2-ads.) (nm)[b]	Co_3O_4 particle size (XRD) (nm)[c]
Co/γ-Al_2O_3	6.3	15.2	13.7
$CoRe/\gamma$-Al_2O_3	10.2	9.4	15.0
Co/SiO_2	5.3	18.1	22.5
$CoRe/SiO_2$	5.8	16.4	20.2
Co/TiO_2	2.3	41.7	41.6
$CoRe/TiO_2$	2.4	40.0	50.8

[a] Co^0 dispersion from H_2 chemisorption at 313 K, assuming adsorption on Co atoms only.
[b] Co^0 particle size calculated from H_2 chemisorption using $d(\mathrm{Co}) = 96/D$.
[c] Co_3O_4 particle size calculated from XRD of calcined catalyst using the most intense peak located at $2\theta = 36.9°$.

Table 4
Pore diameter, pore volume, surface area and porosity

Catalyst	Average pore diameter (nm)	Pore volume (cm^3/g)	Surface area (m^2/g)[c]	Porosity ε (%)[d]
Co/γ-Al_2O_3	6.7[a]	0.34[a]	161	58
$CoRe/\gamma$-Al_2O_3	6.8[a]	0.36[a]	155	59
Co/SiO_2	11[a]	1.0[a]	297	72
$CoRe/SiO_2$	12[a]	1.1[a]	302	74
Co/TiO_2	770[b]	0.77[b]	8	76
$CoRe/TiO_2$	790[b]	0.90[b]	12	80

[a] Calculated from N_2 adsorption measurements.
[b] Calculated from Hg porosimetry measurements.
[c] BET surface area calculated from N_2 adsorption measurements.
[d] Calculated from the measured pore volume.

Re decreased the average Co^0 particle size quite significantly. This is because Re promotes the reduction of cobalt phases interacting strongly with the γ-Al_2O_3 support [17]. The observed effect of Re on the particle size from XRD for the TiO_2-supported catalysts, compared with no effect from H_2 chemisorption, may also be due to cobalt phases interacting with the titania support. If this phase is nonreducible at standard reduction condition, then it does not contribute to the particle size obtained from H_2 chemisorption.

Surface area, pore volume, average pore diameter, and porosity for the different catalysts are given in Table 4. The average pore diameter increased in the same order as the average Co_3O_4 particle sizes. The SiO_2-supported catalysts had a larger average pore diameter (∼12 nm) than the γ-Al_2O_3-supported catalysts (∼7 nm), and the TiO_2-supported catalysts had an average pore diameter close to 800 nm. The pore volume for the γ-Al_2O_3-supported catalysts was significantly smaller than the pore volume for the other catalysts, and thus the porosity was correspondingly smaller as well.

According to the particle sizes obtained from XRD and H_2 chemisorption measurements and the information about the pore structure of the different catalysts, Co^0 and Co_3O_4 particle sizes are controlled by the pore diameter of the support. The same relation between pore diameter and cobalt particle size has been reported previously for various silica supports with pore diameters >3 nm by Khodakov et al. [12,14], Panpranot et al. [8], Saib et al. [16], and Castner et al. [19].

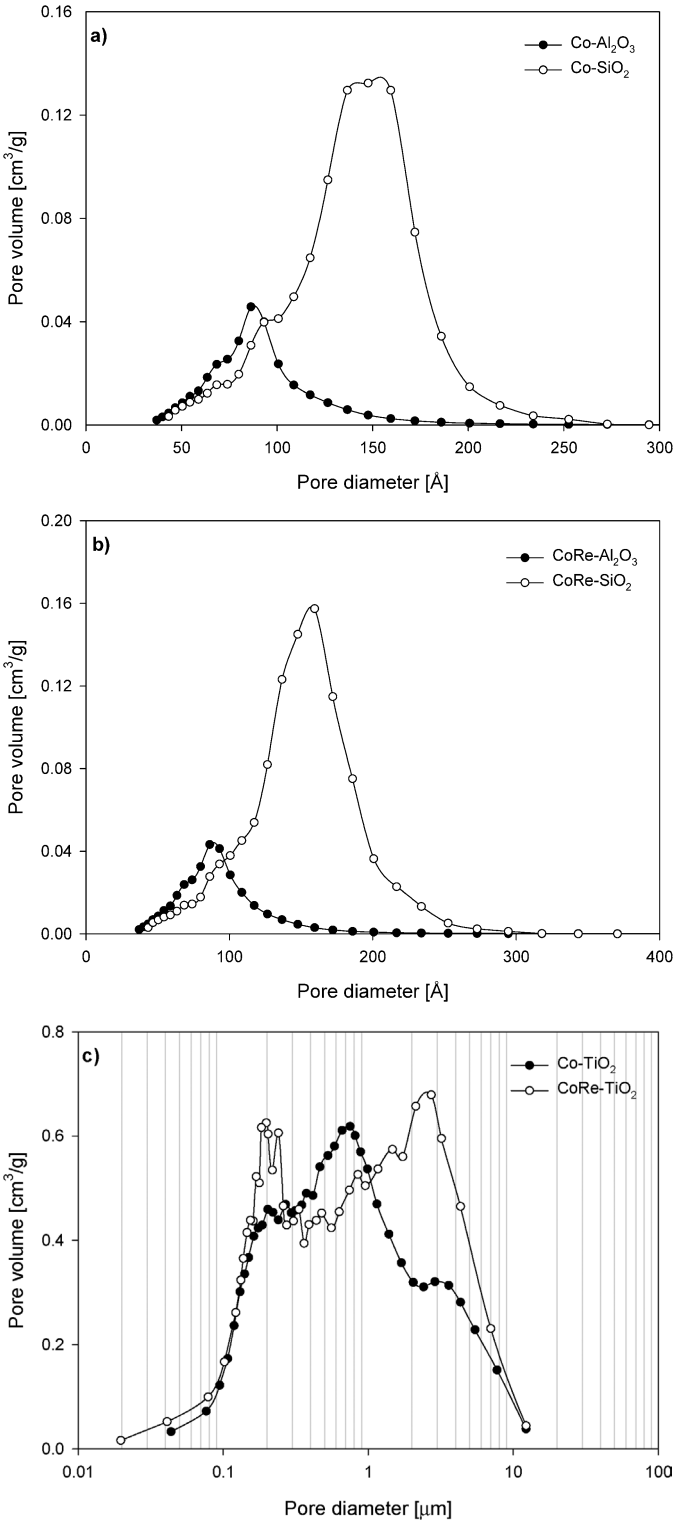

Fig. 3. BJH pore size distribution from the nitrogen desorption curve for (a) Co/γ-Al_2O_3 and Co/SiO_2, (b) CoRe/γ-Al_2O_3 and CoRe/SiO_2, and (c) Co/TiO_2 and CoRe/TiO_2.

Fig. 3 shows the pore size distribution for all of the catalysts. The pore size distribution is broader for the SiO_2 supported catalysts than for the γ-Al_2O_3-supported catalysts (Figs. 3a

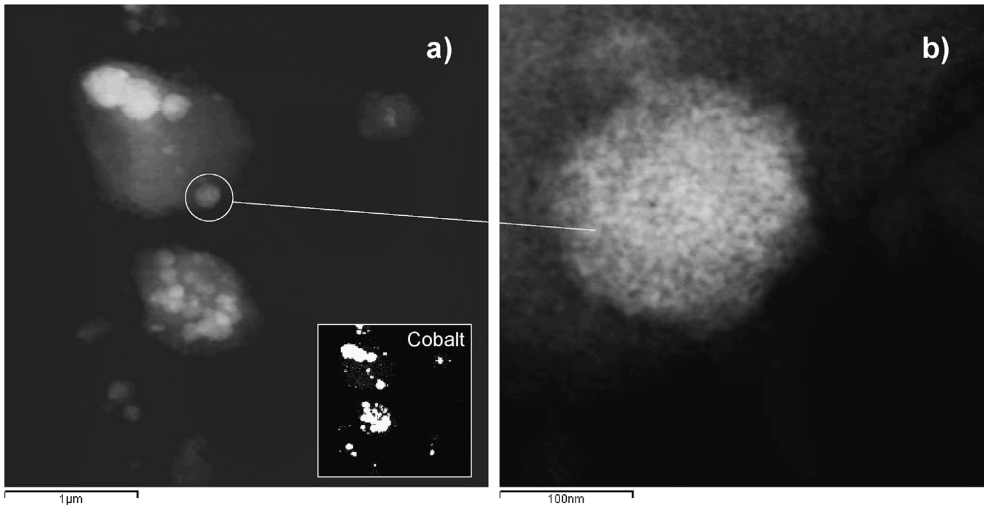

Fig. 4. STEM micrographs of a CoRe/γ-Al_2O_3 sample prepared by sprinkling crushed catalyst on a "holey carbon" film supported on a Ti grid. (a) Low magnification image including an EDS map for determination of Co_3O_4 location. (b) Higher magnification image.

and 3b), and consists of two shoulders on the left side, compared with one shoulder for the γ-Al_2O_3-supported catalysts. Promoting with Re has no major effect on the average pore size or the appearance of the pore size distributions. The pore size distribution (Fig. 3c) of the TiO_2-supported Co and CoRe catalysts differs significantly from that of the other catalysts; the distribution is much broader. The promoted catalyst has a clear bimodal distribution and a larger fraction of both the largest pores and the smallest pores compared with the unpromoted catalyst, which has a larger fraction of the average pores. The pore size distribution for the Co/TiO_2 catalyst consists of three overlapping peaks.

3.2. Electron microscopy

It would have been desirable to be able to perform in situ reduction before conducting the electron microscopy studies; however, this was not possible with the available equipment. For this reason, we attempted to reduce the catalyst and then passivate it using 0.5% O_2 in N_2 before exposing it to air. However, XRD studies of the samples immediately after the passivation procedure showed that the major part of the cobalt oxidized quite rapidly to mainly Co_3O_4, with no traces of Co^0 found. Thus the electron microscopy studies were carried out on catalysts in their calcined state. To obtain good electron microscope images, the samples must be specially prepared to a thickness that allows electrons to transmit through the sample. The two preparation techniques used were described above. STEM annular dark-field images of samples prepared by method one (PM1) are shown in Figs. 4–9, and TEM bright-field images of one γ-alumina sample prepared by method two (PM2) are shown in Fig. 10.

Electron diffraction patterns of all of the catalysts confirm that cobalt is present as Co_3O_4 on the catalysts in their calcined state. Fig. 4 shows dark-field STEM micrographs of CoRe/γ-Al_2O_3. The smaller image inside the large images is an EDS map showing the distribution of cobalt in the micrograph image. In Fig. 4a, Co_3O_4 appears as bright, spherical clusters on the amorphous γ-alumina support, which appears as gray regions. The higher-magnification image in Fig. 4b shows that the Co_3O_4 cluster consists of many smaller Co_3O_4 particles. The contrast is not sufficiently clear to allow a statistical count of the particle sizes, but they are in approximately the 7–25 nm range. The Co_3O_4 cluster sizes observed were distributed at 70–400 nm. The rhenium present is difficult to detect, but EDS suggests that some rhenium is evenly distributed throughout the support, although a large part of rhenium is associated with the cobalt. STEM images of Co/γ-Al_2O_3 showed similar Co_3O_4 cluster sizes and Co_3O_4 particle sizes. STEM analysis did not detect any obvious differences in Co_3O_4 particle size between the rhenium promoted and unpromoted cobalt γ-alumina catalysts, in agreement with the XRD results. Strong interactions between the smallest cobalt particles and the support exist on γ-alumina-supported catalyst. Re is known to enhance the degree of reduction of these cobalt species in strong interaction with the support. The catalysts are reduced in the H_2 chemisorption studies, and this difference in degree of reduction for Co/γ-Al_2O_3 and CoRe/γ-Al_2O_3 is included. For the XRD and STEM studies, the catalysts are not reduced, and the difference in degree of reduction for the two catalysts is not taken into account. This is the reason why an effect of Re on the particle size is observed from the H_2 chemisorption studies, whereas no effect is seen from XRD and STEM.

STEM images of the Co/SiO_2 catalyst are presented in Figs. 5 and 6. As for the γ-Al_2O_3-supported catalysts, Co_3O_4 appears as clusters (Fig. 5a), mainly spherical in shape but with some oval and even hexagonal clusters. There is a wide distribution in Co_3O_4 cluster size on the silica support, ranging between 40 and 700 nm. It is not easy to detect the Co_3O_4 particle sizes from the image in Fig. 5b, in which several Co_3O_4 particles are very closely connected. However, from the micrograph images and especially from the inserted EDS maps of the smallest Co_3O_4 clusters, as shown in Fig. 6, it is possible to roughly distinguish Co_3O_4 particles from the silica support. Thus, from the smallest clusters, the Co_3O_4 particle sizes are found to be in the 10–35 nm range. The particles seem to have

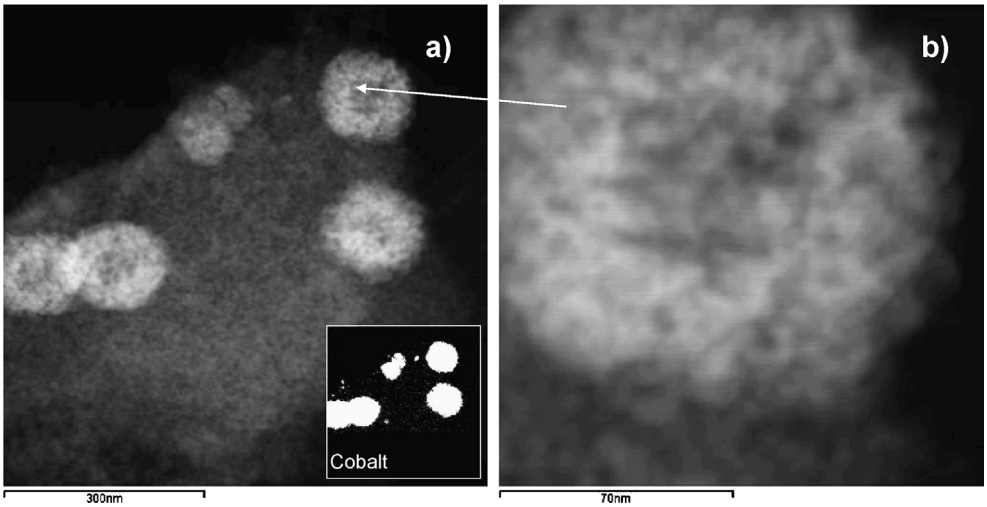

Fig. 5. STEM micrographs of a Co/SiO_2 sample prepared by sprinkling crushed catalyst on a "holey carbon" film supported on a Ti grid. (a) Low magnification image and (b) higher magnification image.

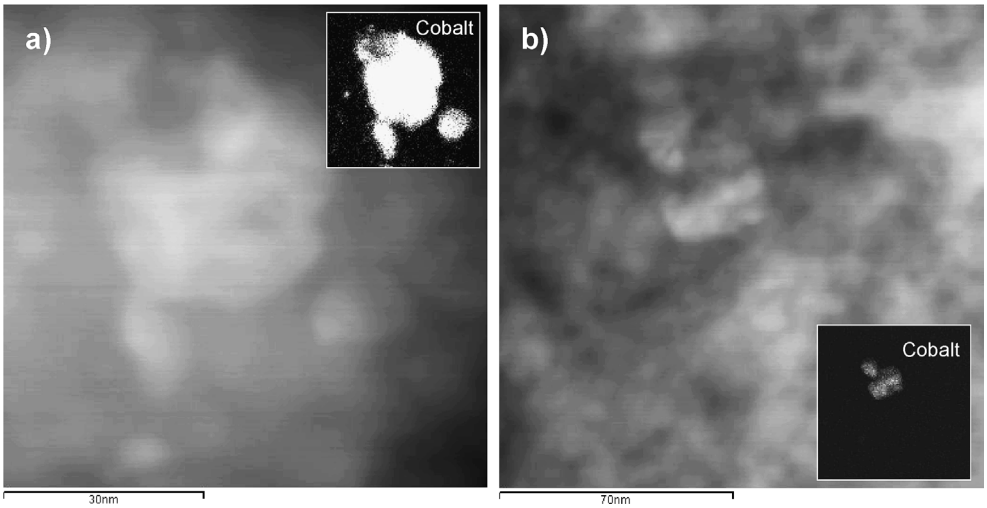

Fig. 6. STEM micrographs of a Co/SiO_2 sample prepared by sprinkling crushed catalyst on a "holey carbon" film supported on a Ti grid. Both (a) and (b) are high magnification images including EDS maps for determination of Co_3O_4 particle sizes.

different shapes; most are spherical, but some drop-like oval particles are also seen. The broader distribution of cluster sizes and particle sizes of Co_3O_4 observed on the silica support compared with the γ-alumina support is consistent with the broader pore size distributions for the silica-supported catalysts. It appears that larger pores result in larger clusters of Co_3O_4 during drying and calcination, in addition to larger Co_3O_4 and Co^0 particles.

No significant differences in shape, Co_3O_4 cluster size, or Co_3O_4 particle size were found between the $CoRe/SiO_2$ and Co/SiO_2 catalysts. The fraction of larger agglomerates found on the silica-supported catalysts is probably due to the proportion of larger pores for the silica catalysts compared with the γ-alumina catalyst. Saib et al. [16] also found that an increase in average pore size from 40 to 150 Å for silica-supported catalysts led to an increase in the average cluster size.

The STEM images of cobalt supported on titania appear different from those of cobalt supported on silica and γ-alumina, and the contrast between Co_3O_4 and titania is also much clearer. Indeed, it is easier to make a distinction between Co_3O_4 and titania at higher magnifications than at lower magnifications. Micrographs of the Co/TiO_2 catalyst are shown in Figs. 7a, 7b and 8a. On the small EDS map inserted into Fig. 7a, Co_3O_4 appears as discrete particles that look almost sponge-like. Unlike the γ-alumina- and silica-supported catalysts, Co_3O_4 appears as crystalline particles distributed relatively evenly over the support. Particle shape varies significantly, with some appearing hexagonal (Fig. 7b) and others looking like peanuts or droplets. These are the same structures observed by Jabłoński et al. [59] for low-surface area silica. These authors found that on high-surface area silica, the Co_3O_4 particles exists as agglomerates, whereas for low-surface area silica, with larger pores, the Co_3O_4 phase is more evenly distributed. Also, Castner et al. [19] have reported that Co_3O_4 particles are clustered together on silica with small pores, but not on silica with large pores.

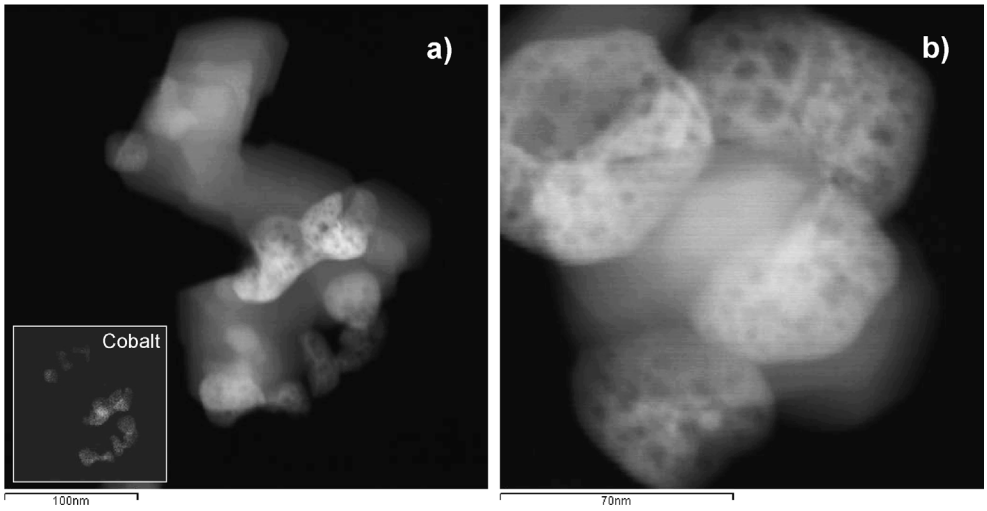

Fig. 7. STEM micrographs of a Co/TiO_2 sample prepared by sprinkling crushed catalyst on a "holey carbon" film supported on a Ti grid. (a) High magnification image including an EDS map for determination of Co_3O_4 location. (b) High magnification images showing the size of Co_3O_4 particles.

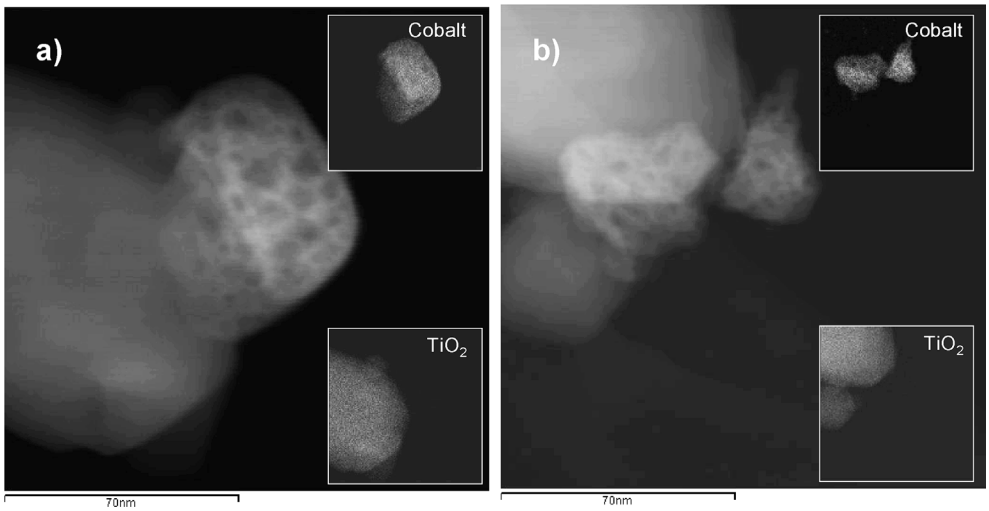

Fig. 8. High magnification STEM micrograph of (a) a Co/TiO_2 sample and (b) a $CoRe/TiO_2$ sample, both prepared by sprinkling crushed catalyst on a "holey carbon" film supported on a Ti grid.

Fig. 8b is an annular dark-field image of $CoRe/TiO_2$ with inserted EDS maps showing the cobalt-containing and titania-containing areas. The Co_3O_4 particles are generally found on the edge of the titania grains. Measuring particle size is not easy, because of the particles' irregular shapes. However, based on the dimension in the elongated direction, the Co_3O_4 particle size is estimated as 30–80 nm for the Co/TiO_2 catalyst and 30–70 nm for the $CoRe/TiO_2$ catalyst. For the rhenium-promoted catalyst, the Co_3O_4 particle sizes seem slightly smaller, in contrast to the results from XRD. For calculating particle sizes from XRD, spherical particles are assumed. This assumption obviously is not valid for the cobalt particles supported on TiO_2, and may be one reason for the differences in Co_3O_4 particle sizes derived from XRD, STEM, and H_2 chemisorption. For both the silica- and the γ-alumina-supported catalysts, the Co_3O_4 particle sizes obtained from XRD are within the particle size distribution range obtained from the STEM images.

As stated above, cobalt has been found to exist as clusters on high-surface area silica and as single particles more evenly distributed on low-surface area silica. For comparison, a CoRe catalyst supported on α-alumina (a low-surface area support) was also included in the STEM study. This catalyst has a BET surface area of 23.5 m^2/g, an average pore diameter of 0.15 µm, and a pore volume of 0.54 cm^3/g. Micrographs of the $CoRe/\alpha$-Al_2O_3 catalyst are shown in Fig. 9. Co_3O_4 shows slightly brighter contrast, and, as on TiO_2, Co_3O_4 appears as discrete particles that appear almost porous. The particles are relatively evenly distributed over the support, and the shape of the particles differs significantly. A relatively broad particle distribution is found, ranging from 10 to 100 nm; however, most of the particles are in the 20–50 nm range (length in the elongated direction).

For the promoted γ-Al_2O_3, SiO_2, and TiO_2 catalysts, analytical elemental analysis of random cobalt-containing areas was

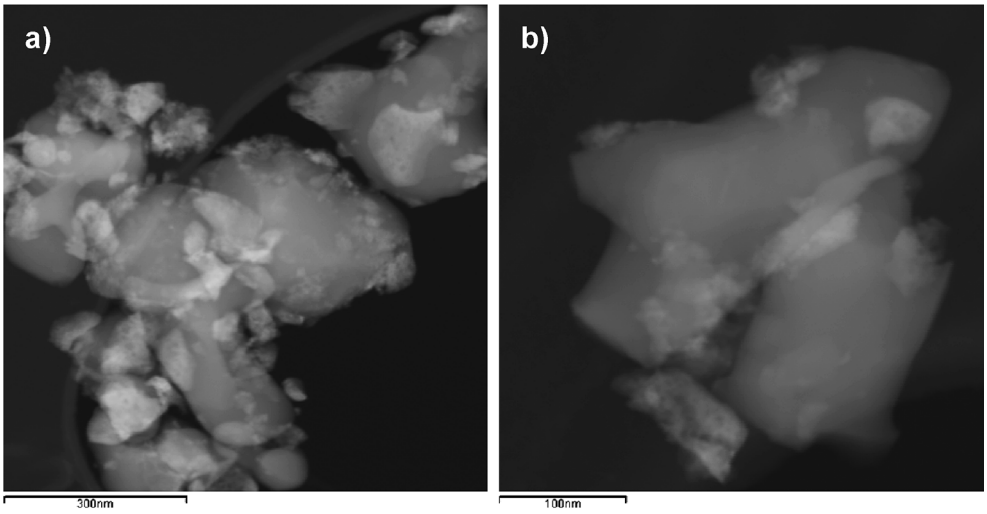

Fig. 9. STEM micrographs of a Co/α-Al_2O_3 sample prepared by sprinkling crushed catalyst on a "holey carbon" film supported on a Ti grid. (a) Low magnification image and (b) higher magnification image.

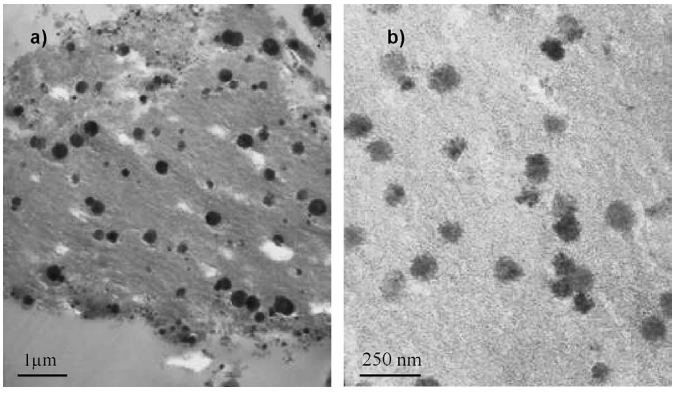

Fig. 10. TEM micrographs of a Co/γ-Al_2O_3 sample prepared by ultramicrotomy. (a) Low magnification image and (b) higher magnification image showing different cluster sizes.

performed to detect the quantity of rhenium located in cobalt-rich areas. The concentration of rhenium was 1.3–3.1 at%, with an average value of 2.1 at% for the SiO_2 catalyst. For the TiO_2-supported catalysts, the cobalt-containing areas contained 0.5–3.8 at% Re, with an average value of 1.9 at%. The amount of Re in the γ-Al_2O_3-supported catalyst was 0.5–2.6 at%, with an average value of 1.2 at%.

Bright contrast in an annular dark-field image can be due to higher average atomic number or to uneven sample thickness. Because of this relatively complicated contrast observed on some of the STEM images prepared by PM1, samples were also prepared by another method. The main purpose was to create thinner samples, with even, parallel, surfaces, to prevent thickness differences from influencing the contrast between cobalt oxide and the support. In some cases PM2 was a more promising preparation method than PM1. Fig. 10 shows bright-field TEM images of the Co/γ-Al_2O_3 catalyst; here Co_3O_4 is represented by the dark spots in the micrograph. As in Fig. 4, here Co_3O_4 appears as clusters, and in this case it is possible to locate many clusters in one image, making the counting of cluster sizes much easier. The average cluster size was in the same range as before, 70–400 nm. The embedded sections of the sample tended to charge under the electron beam and fell from the resin if the electron beam current was too high, limiting the detailed analysis of microtomed samples. Voß et al. [13] also prepared samples for TEM following the same principles, embedding the catalyst in epoxy resin followed by ultramicrotomy, and found that on a silica support, contrast cobalt oxide clusters were easily distinguished from the support. However, they found that it was not possible to distinguish between cobalt oxide and the support on alumina and titania supports. Okamoto et al. [43], Sun et al. [44], and Castner et al. [19] also obtained valuable information on Co/SiO_2 catalysts by TEM using preparation method PM2.

The TEM studies demonstrated that on silica (average pore size ∼120 Å) and γ-alumina (average pore size ∼70 Å), Co_3O_4 appears in agglomerates of different sizes created during the drying and calcination process. On titania, which has a much larger average pore size, Co_3O_4 emerges mostly as larger single particles. The Co_3O_4 particles will probably exist as agglomerates up to a certain pore size, beyond which no agglomeration will occur. This is the case both in the present study and in previous studies on small- and large-pore silicas [16,19,59].

The average Co_3O_4 particle sizes on γ-alumina- and silica-supported catalysts determined by XRD and STEM are larger than the average pore sizes. This means that a large fraction of the particles is located not inside single pores, but rather on the outside or occupying adjacent, interconnecting, pore cavities. This may be the reason why Co_3O_4 appears as agglomerates on these two supports. The cobalt precursor is mobile during drying and calcination and thus may diffuse in the pores, forming clusters. The drying and calcination steps are very important during catalyst preparation [6,52–55]. Because of the higher porosity of the silica support compared with the γ-alumina support, the pores are possibly more closely connected. This may enhance the possibility of diffusion into adjacent pore cavities and decrease the distance between the cobalt particles, which in turn may further increase the probability of cluster growth, due to shorter diffusion distances, and be the reason for the larger

Table 5
Hydrogen consumption from TPR and extent of reduction calculated from TPR and O_2-titration

Catalyst	H:Co[a,b] calcined catalyst	H:Co[a] reduced catalyst	Extent of reduction	
			TPR	O_2-titration[c]
Co/γ-Al_2O_3	2.4	0.89	54	53
CoRe/γ-Al_2O_3	2.4	0.17	79	61
Co/SiO_2	2.4	0.12	85	65
CoRe/SiO_2	2.3	0.02	86	66
Co/TiO_2	2.7	0.01	100	69
CoRe/TiO_2	2.9	0.02	105	71

[a] mol H/mol Co assuming negligible consumption of H_2 for reduction of Re_2O_7. Complete reduction of Co_3O_4 requires 2.67 moles of H per mole of Co.
[b] The uncertainty ($\pm 2\sigma$) is calculated to be ± 0.1 based on standard deviation from multiple experiments.
[c] The uncertainty ($\pm 2\sigma$) is calculated to be $\pm 1\%$ based on standard deviation from multiple experiments.

clusters observed on silica compared with γ-alumina. However, the internal structure of these supports remains incompletely understood.

The titania and α-alumina supports have much larger pores than silica and γ-alumina, and larger Co_3O_4 particles are formed (Fig. 7). The average Co_3O_4 particle size is smaller than the average pore size, meaning that in this case the particles are probably located inside single pores. The larger particles do not easily migrate on the support surface in the pores or on the surface of the particles, and no agglomeration take place. This may also be the reason why Co_3O_4 particles located on the edge of titania grains were found, whereas for the silica and γ-alumina catalysts, support was observed beneath the Co_3O_4 particles in all cases.

3.3. Degree of reduction

The degree of reduction is an important parameter, containing information about the interaction with the support. A corrected dispersion can also be calculated based on the degree of reduction [17]. The degree of reduction was obtained both from TPR and O_2 titration measurements; the values are given in Table 5. When TPR is used to estimate the degree of reduction, reduction of Co_3O_4 to Co^0, requiring 2.67 mol of H per mol of cobalt, is assumed. For the calcined γ-alumina-supported catalysts, some of the cobalt remains as cobalt nitrate after calcination, which is taken into account in the calculations from TPR. The degree of reduction from O_2 titration is based on the assumption of complete oxidation of Co^0 to Co_3O_4.

With the exception of Co/γ-Al_2O_3, the values from O_2 titration are systematically lower than those from TPR. Based on repeating measurements, the uncertainty in the hydrogen consumption from TPR (H:Co ratio in Table 5) for the calcined catalysts is $\pm 4\%$. This uncertainty is also present for the degree of reduction. The extent of reduction from O_2 titration has an uncertainty of about $\pm 2\%$; however, within the estimated errors, the values from TPR are still higher than the values from O_2 titration. Kodakov et al. [12,52] stated that in inert atmospheres at temperatures $>350\,^\circ$C, CoO could be more stable than Co_3O_4. If this is the case, then the assumption of complete oxidation of Co^0 to Co_3O_4 is not valid, and the degree of reduction from O_2 titration is too low. The extent of reduction for the Co/γ-Al_2O_3 catalyst from TPR is in good agreement with that from O_2 titration.

For titania-supported noble metal catalysts, strong metal-support interactions (SMSIs) are observed when the reduction temperature is $>300\,^\circ$C [74], and the reduction procedure may reduce the support to form a suboxide (TiO_x), [75]. Thus the hydrogen consumption during TPR for the titania-supported catalysts may be due to reduction of the support, in addition to reduction of Co_3O_4. This could explain the high extent of reduction calculated for these systems, which is indeed higher than the theoretical value for CoRe/TiO_2.

The degree of reduction from TPR and O_2 titration increases in the order $Al_2O_3 < SiO_2 < TiO_2$. The reducibility reflects the extent of the metal–support interaction. Jacobs et al. [7] found the metal–support interaction to be in the order γ-$Al_2O_3 > TiO_2 > SiO_2$. However, for titania, the degree of interaction depends strongly on the TiO_2 phase. It has been found that the metal–support interactions are weaker for rutile titania than for anatase titania [15,74]. The titania used in this work is mainly rutile, as found by XRD (Fig. 2). Furthermore, the water produced during TPR may have an influence on the metal–support interaction and on the reducibility of γ-alumina- and titania-supported catalysts. For Co supported on titania, the evolution of water vapor during reduction and the reduction itself resulted in a rather large decrease in reducibility, indicating the formation of nonreducible "Co-titanate" [58]. Also for Co supported on alumina, the presence of water vapor during reduction and the reduction itself have been found to retard the reducibility, to a larger extent than for Co/TiO_2 [56,57,61]. This is explained by increased Co–aluminate interaction and/or formation of nonreducible cobalt compounds. For Co/SiO_2, it has been found that the formation of cobalt–support compounds that are nonreducible at $<900\,^\circ$C occurs only when hydrothermal treatment is carried out on the reduced catalysts [76]. Thus the reduction process itself, as well as the procedure for dealing with the water produced during reduction, are important to reducibility. Different metal–support interactions formed for the different supports and various techniques during the reduction may partially explain the observed dissimilarities.

Borg et al. [77] recently determined the extent of reduction by X-ray absorption spectroscopy (XAS) measurements for the same series of Re-promoted catalysts. The degree of reduction increased in the order CoRe/γ-Al_2O_3 < CoRe/TiO_2 < CoRe/SiO_2 and was 63, 75, and 85% from X-ray absorption near-edge spectroscopy (XANES) and 65, 75, and 79% from EXAFS, respectively. The consistency between XANES and EXAFS results was found to be within the limits of experimental error. Nonetheless, the results are somewhat higher than the O_2 titration values, especially for the silica-supported catalyst. The discrepancy from the O_2 titration values may be due to the incomplete oxidation described above. The extent of reduction from TPR for the silica-supported catalysts is in good agreement with the results from XAS, but for the γ-alumina- and titania-supported catalysts, the values from XAS are lower than

those from TPR. It should be noted, however, that the reduction in XAS was carried out at 400 °C, whereas for O_2 titration and TPR of reduced catalysts, the samples were prereduced at 350 °C. A higher reduction temperature may increase the degree of reduction by reducing cobalt oxide, which is nonreducible at 350 °C [7]. However, at the same time a higher reduction temperature in XAS may result in a higher degree of metal–support interaction, and thus lower reducibility. This is particularly true for the γ-alumina- and titania-supported catalysts. As stated above, the reduction process decreases the reducibility for both titania- and alumina-supported catalysts due to metal–support compound formation.

3.4. Structural parameter and mass transfer limitations

Activity and selectivity data for the γ-Al_2O_3-, SiO_2-, and TiO_2-supported catalysts have been presented previously [17], and results obtained at 40–45% conversion are given in Table 1. Activity and selectivity data obtained shortly after 20% water addition are reviewed in Table 2. Activity and selectivity data for the sample using α-Al_2O_3 as the support have also been reported previously [10,18].

Diffusion is also an important phenomenon in FT synthesis. Although the reactants are in the gas phase, the support pores are filled with liquid products, and diffusion in the liquid phase is several orders of magnitude slower than in the gas phase. Reactants and products must be transported to and from the catalytic active sites; thus the two major diffusion limitations are reactant arrival and product removal. Iglesia et al. [21] derived a model for the FT process based on reaction and diffusion in the catalyst pores. The analysis is based on a structural parameter χ [21],

$$\chi = \frac{R_0^2 \varepsilon \theta_M}{r_p}, \tag{2}$$

where R_0 is the diffusion length, ε is porosity, θ_M is site density, and r_p is the mean pore diameter. The χ values for the catalysts involved in this study are included in Table 1.

According to the model proposed by Iglesia et al., C_{5+} selectivity will increase due to olefin readsorption up to a χ value of about 1000×10^{16} m^{-1} and then decrease because of unfavorable H_2/CO ratios [21]. In the catalytic systems studied previously by us [17], such behavior was not observed. The C_{5+} selectivity remains constant up to χ values of about 1000×10^{16} m^{-1}, after which it decreases.

For the catalysts involved in Table 1, the χ values are all in the range 7–52 $\times$ 10^{16} m^{-1}. For diffusion-limited CO arrival to become valid, structural parameters larger than 1000×10^{16} m^{-1} are needed [21,64]. To obtain such values with the present catalysts, required pellet sizes are about 0.3 mm for the γ-alumina-supported catalysts, 0.7 mm for the silica-supported catalysts, and 0.9 mm for the titania-supported catalyst. Because pellet sizes of 53–90 μm are used in the present study, the reaction rates and selectivities should not be limited by diffusion of CO to the active sites.

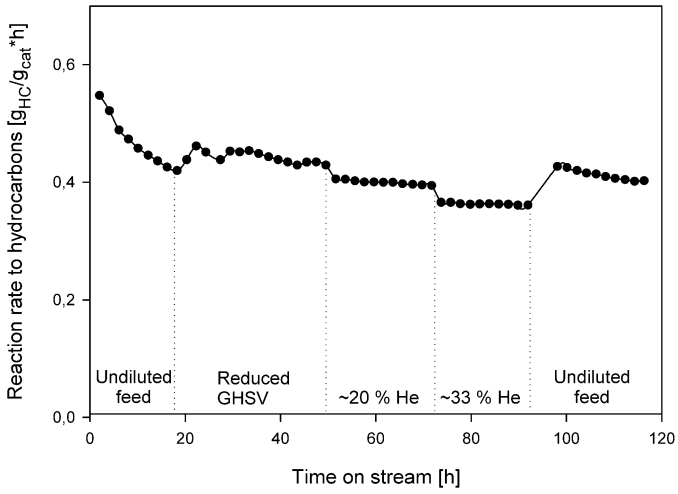

Fig. 11. The effect of reducing the partial pressure of H_2 and CO, by co-feeding helium at constant reactor pressure, on the observed reaction rate for formation of hydrocarbons for CoRe/γ-Al_2O_3. $H_2/CO = 2.1$, $P_{Tot} = 20$ bar, $T = 210$ °C.

3.5. Catalytic behavior contra pore sizes, particle sizes, and cluster sizes

The previous studies carried out in a fixed-bed reactor at 20 bar, 210 °C, and $H_2/CO = 2.1$ [17] showed that with increasing conversion, the observed rate increased for the silica- and titania-supported catalysts. The rate increased even further with the addition of 25% water. For the γ-alumina-supported catalysts, only a slight increase in activity was observed as the conversion increased, and the catalysts deactivated with increasing time on stream. Increased deactivation was observed with the addition of 25% water. For the silica-supported catalysts, an increase in the partial pressure of water inside the reactor also resulted in rapid deactivation. Larger amounts of water (33%) led to decreased activity and increased deactivation for all catalysts.

The reason for adding external water is to simulate high conversion, wherein a large amount of water is formed. The total pressure is kept constant as water is added; however, the partial pressures of H_2 and CO are reduced. Thus the effect of reduced partial pressure of H_2 and CO on the reaction rate and selectivity was considered by running experiments over the CoRe/γ-Al_2O_3 catalyst, replacing the water with the addition of helium. A detailed description of the experimental setup has been given previously [17]. The experiments were performed in a fixed-bed reactor at 20 bar, 210 °C, and a H_2/CO ratio of 2.1. The testing involved five periods. In period I, 200 Nml/min of synthesis gas was added; in period II, the GHSV was adjusted to give 40–45% conversion; and in periods III and IV, 20% and 33% He were added, respectively. During period V, the same conditions as in period II were used.

The reaction rate to hydrocarbons as a function of time on stream during the different periods is shown in Fig. 11. The results show that when 20% He was added, the observed reaction rate dropped by 5.5%. The reaction rate was further reduced by 7% when 33% He was added. The activity returned to the same level as before He addition when the He flow was removed.

This implies that for the γ-alumina-supported catalysts, some of the decrease in the reaction rate as water was added was due to the reduced partial pressures of H_2 and CO. If the experiments with He on CoRe/γ-Al_2O_3 were also representative for the silica- and titania-supported catalysts, then the increase in reaction rate in these systems as 20% water is added would have been slightly higher if the partial pressures had remained constant. The decrease in observed reaction rate with the addition of 33% water for all of the catalyst systems is, according to the results shown in Fig. 11, due to a decrease in the partial pressures of H_2 and CO in addition to the deactivation. Another interesting point is that when He was added to the feed, the deactivation rate for CoRe/γ-Al_2O_3 was slower than when no He was added, as observed from Fig. 11.

The smaller cobalt particles and the agglomerates on the γ-alumina- and silica-supported catalysts found on the STEM studies may be the reason for the deactivation in the presence of water. This is because the smaller metal particles are more exposed for the formation of a Co–support interaction and reoxidation. The larger particles and no agglomeration observed for the titania catalysts seem to favor higher stability against deactivation on water exposure. Thus, this tendency for the Co_3O_4 particles to agglomerate during drying and calcination seems to be very important to the catalytic performance. In addition, the location of the particles (i.e., inside a single pore, in the pore mouths, or occupying adjacent pores) may be an important factor in the effect of water and may influence the degree of metal–support interaction. In addition to particle size, particle location, and the tendency to form agglomerates, the different support materials also must be taken into account. The metal–support interactions are dependent on the type of support. It has been found that Co on γ-alumina reoxidizes in the presence of water [63], and that cobalt silicate forms for Co supported on silica [68]. It has been reported that the presence of the rutile phase on titania stabilizes the Co/TiO_2 catalyst by blocking the formation of Co species strongly interacting with the titania support [15].

The C_{5+} selectivity was found to increase with increasing conversion and by increasing the amount of external water for all three supports. The effect of water on C_{5+} selectivity was largest for the TiO_2-supported catalysts and smallest for the γ-Al_2O_3-supported catalysts (Table 2). Fig. 12 shows the effect of reducing the partial pressures of H_2 and CO on the C_{5+} and CH_4 selectivities. No effect is observed on the CH_4 selectivity, and the C_{5+} selectivity increases only slightly (0.5%) as 20% He is added, and a further increase of 0.2% is observed when 33% He is added. However, the increase in C_{5+} selectivity as water is added (3–8.5%) was found to be much higher than 0.5%. This implies that the decrease in the partial pressures of H_2 and CO as water is added has only a limited influence on the selectivities observed.

Water influences the selectivity in different ways. Water inhibits secondary hydrogenation of the primary formed α-olefins [10]. Water has a diluting effect on the catalytic surface and it seems to be important for the carboneous intermediates forming on the surface. Bertole et al. [78] found that water increases the amount of active surface carbon monomers, caused by an

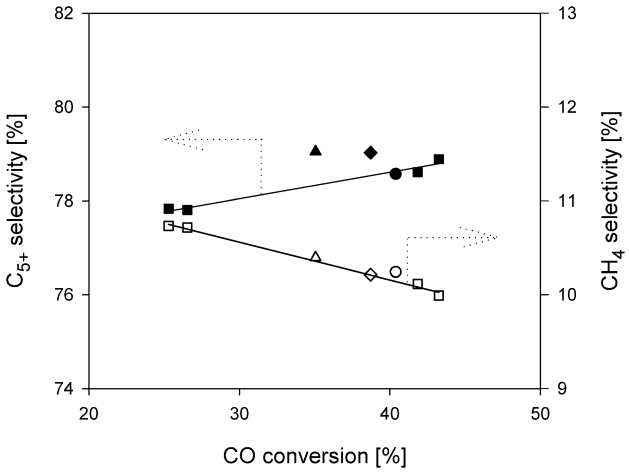

Fig. 12. The effect of reducing the partial pressure of H_2 and CO, by co-feeding helium at constant reactor pressure, on C_{5+} selectivity (filled symbols) and CH_4 selectivity (open symbols) for CoRe/γ-Al_2O_3. Before He addition (■, □), ∼20% He added (◆, ◇), ∼33% He added (▲, △) and after He addition (●, ○).

acceleration of the CO dissociation rate without a matching reactivity increase in the downstream hydrocarbon synthesis steps. In turn, the monomer dependencies in the FT synthesis mechanism explain the lower methane selectivity and higher-molecular weight products observed at increased water concentration. The effect of water may also be related to the location and availability of the particles on the support.

Larger pores, and thus larger metal particles, have been found to favor higher C_{5+} selectivities, particularly when external water is added (Table 2) [17]. Separate studies of the hydrogenation of propene on FT catalysts have also shown that hydrogenation is suppressed on larger particles [10]. For a series of CoRe/γ-Al_2O_3 catalysts with different metal particle sizes, a linear relationship between C_{5+} selectivity and particle size was obtained [79]. Comparing γ-Al_2O_3, α-Al_2O_3, and TiO_2 showed the same relationship between C_{5+} selectivity and particle size [10]. In the case of γ-alumina and silica, the Co_3O_4 particles are located in clusters, and cluster size also could be important to catalytic behavior. The STEM studies involve cobalt oxide, and not the metal in its reduced state. Furthermore, STEM studies of used catalysts have not been performed, and detailed information about the working catalyst is lacking.

Comparing the C_{5+} selectivities for the unpromoted catalysts at dry conditions (Table 1) shows that there is a small difference between the different supports. However, for the Re-promoted counterparts, the silica- and titania-supported catalysts result in notably higher C_{5+} selectivities than the γ-alumina-supported catalyst. It can be speculated that this may be due to the slightly closer contact between rhenium and cobalt on the silica- and titania-supported catalysts than on the γ-alumina-supported catalyst, as found from the element analytical analysis in STEM.

4. Conclusions

A series of unpromoted and Re-promoted cobalt catalysts supported on γ-Al_2O_3, SiO_2, and TiO_2 was studied using dif-

ferent characterization techniques. A CoRe/α-Al_2O_3 catalyst was included in the STEM study for comparison.

XRD and STEM showed that cobalt exists as Co_3O_4 on the catalysts in their calcined state. Pore structures were found to greatly influence the size, shape, and appearance of the cobalt particles. On the small-pore γ-Al_2O_3 and SiO_2 supports, Co_3O_4 exists as clusters (agglomerates of smaller particles) with rather broad cluster size distribution, whereas on the wide-pore TiO_2 and α-Al_2O_3 supports, Co_3O_4 was found as single particles, evenly distributed. The average Co_3O_4 particle size increases with increasing pore diameter of the support. The Co_3O_4 cluster sizes were found to be larger on SiO_2 compared with the γ-Al_2O_3 support.

From this STEM study and the earlier studies on low- and high-surface area silica, it can be concluded that on high-surface area supports, cobalt tends to agglomerate into clusters. For low-surface area supports, the cobalt is more evenly distributed, and is found as single crystalline particles. Rhenium seems to be in close contact with the cobalt, and more so for CoRe supported on TiO_2 and SiO_2 than on γ-Al_2O_3. The pore structure has a significant effect on the size, location, shape, and appearance of the cobalt particles.

Acknowledgments

Financial support was provided by the Norwegian Research Council. The authors thank Lehigh University for allowing the use of their microscope equipment.

References

[1] E. Iglesia, S.L. Soled, R.A. Fiato, J. Catal. 137 (1992) 212.
[2] E. Iglesia, Appl. Catal. A 161 (1997) 59.
[3] R.C. Reuel, C.H. Bartholomew, J. Catal. 85 (1984) 78.
[4] R. Riva, H. Miessner, R. Vitali, G. Del Piero, Appl. Catal. A 196 (2000) 111.
[5] R. Riva, H. Miessner, G. Del Piero, B. Rebours, M. Roy, Stud. Surf. Sci. Catal. 119 (1998) 203.
[6] E. van Steen, G.S. Sewell, R.A. Makhothe, C. Micklethwaite, H. Manstein, M. de Lange, C.T. O'Connor, J. Catal. 162 (1996) 220.
[7] G. Jacobs, T.K. Das, Y. Zhang, J. Li, G. Racoillet, B.H. Davis, Appl. Catal. A 233 (2002) 263.
[8] J. Panpranot, J.G. Goodwin Jr., A. Sayari, J. Catal. 211 (2002) 530.
[9] S. Eri, K.J. Kinnari, D. Schanke, A.-M. Hilmen, PCT Int. Appl. WO 2002047816 (2002).
[10] C. Aaserud, A.-M. Hilmen, E. Bergene, S. Eri, D. Schanke, A. Holmen, Catal. Lett. 94 (2004) 171.
[11] W.J. Wang, Y.W. Chen, Appl. Catal. 77 (1991) 223.
[12] A.Y. Khodakov, A. Griboval-Constant, R. Bechara, V.L. Zholobenko, J. Catal. 206 (2002) 230.
[13] M. Voß, D. Borgmann, G. Wedler, J. Catal. 212 (2002) 10.
[14] A.Y. Khodakov, R. Bechara, A. Griboval-Constant, Appl. Catal. A 254 (2003) 273.
[15] B. Jongsomjit, C. Sakdamnuson, P. Praserthdam, Mater. Chem. Phys. 89 (2004) 395.
[16] A.M. Saib, M. Claeys, E. van Steen, Catal. Today 71 (2002) 395.
[17] S. Storsæter, Ø. Borg, E.A. Blekkan, A. Holmen, J. Catal. 231 (2005) 405.
[18] D. Schanke, S. Eri, E. Rytter, C. Aaserud, A.-M. Hilmen, O.A. Lindvåg, E. Bergene, A. Holmen, Stud. Surf. Sci. Catal. 147 (2004) 301.
[19] D.G. Castner, P.R. Watson, I.Y. Chan, J. Phys. Chem. 93 (1989) 3188.
[20] E. Iglesia, S.L. Soled, R.A. Fiato, US Patent 4 738 948 (1988).
[21] E. Iglesia, S.C. Reyes, R.J. Madon, S.L. Soled, Adv. Catal. 39 (1993) 221.
[22] J. Zhang, J. Chen, J. Ren, Y. Sun, Appl. Catal. A 243 (2003) 121.
[23] J. Zhang, J. Chen, J. Ren, Y. Li, Y. Sun, Fuel 82 (2003) 581.
[24] G.R. Moradi, M.M. Basir, A. Taeb, A. Kiennemann, Catal. Commun. 4 (2003) 27.
[25] A. Feller, M. Claeys, E. van Steen, J. Catal. 185 (1999) 120.
[26] F. Rohr, A. Holmen, K.K. Barbo, P. Warloe, E.A. Blekkan, Stud. Surf. Sci. Catal. 119 (1998) 107.
[27] F. Rohr, O.A. Lindvåg, A. Holmen, E.A. Blekkan, Catal. Today 58 (2000) 247.
[28] A.M. Hilmen, D. Schanke, A. Holmen, Catal. Lett. 38 (1996) 143.
[29] D. Schanke, S. Vada, E.A. Blekkan, A.M. Hilmen, A. Hoff, A. Holmen, J. Catal. 156 (1995) 85.
[30] A.M. Hilmen, D. Schanke, K.F. Hanssen, A. Holmen, Appl. Catal. A 186 (1999) 169.
[31] A. Hoff, E.A. Blekkan, A. Holmen, D. Schanke, Stud. Surf. Sci. Catal. 75 (1993) 2067.
[32] G.W. Huber, C.H. Bartholomew, Stud. Surf. Sci. Catal. 136 (2001) 283.
[33] G.W. Huber, S.J.M. Butala, M.L. Lee, C.H. Bartholomew, Catal. Lett. 74 (2001) 45.
[34] G. Jacobs, P.M. Patterson, Y. Zhang, T. Das, J. Li, B.H. Davis, Appl. Catal. A 233 (2002) 215.
[35] A. Kogelbauer, J.G. Goodwin Jr., R. Oukaci, J. Catal. 160 (1996) 125.
[36] J. Li, G. Jacobs, Y. Zhang, T. Das, B.H. Davis, Appl. Catal. A 223 (2002) 195.
[37] C.H. Mauldin, D.E. Varnado, Stud. Surf. Sci. Catal. 136 (2001) 417.
[38] T.K. Das, G. Jacobs, P.M. Patterson, W.A. Conner, J. Li, B.H. Davis, Fuel 82 (2003) 805.
[39] C.L. Bianchi, Catal. Lett. 76 (2001) 155.
[40] S.L. Soled, E. Iglesia, R.A. Fiato, J.E. Baumgartner, H. Vroman, S. Miseo, Top. Catal. 26 (2003) 101.
[41] J. Panpranot, S. Kaewkun, P. Praserthdam, J.G. Goodwin Jr., Catal. Lett. 91 (2003) 95.
[42] M. Kraum, M. Baerns, Appl. Catal. A 186 (1999) 189.
[43] Y. Okamoto, K. Nagata, T. Adachi, T. Imanaka, K. Inamura, T. Takyu, J. Phys. Chem. 95 (1991) 310.
[44] S. Sun, N. Tsubaki, K. Fujimoto, Appl. Catal. A 202 (2000) 121.
[45] J. Li, N.J. Coville, S. Afr. J. Chem. 56 (2003) 1.
[46] G. Bian, T. Mochizuki, N. Fujishita, H. Nomoto, M. Yamada, Energy Fuels 17 (2003) 799.
[47] W.-P. Ma, Y.-J. Ding, L.-W. Lin, Ind. Eng. Chem. Res. 43 (2004) 2391.
[48] M.A. Stranick, M. Houalla, D.M. Hercules, J. Catal. 104 (1987) 396.
[49] S.W. Ho, J.M. Cruz, M. Houalla, D.M. Hercules, J. Catal. 135 (1992) 173.
[50] B. Ernst, S. Libs, P. Chaumette, A. Kiennemann, Appl. Catal. A 186 (1999) 145.
[51] A. Barbier, A. Hanif, J.-A. Dalmon, G.A. Martin, Appl. Catal. A 168 (1998) 333.
[52] A.Y. Khodakov, J. Lynch, D. Bazin, B. Rebours, N. Zanier, B. Moisson, P. Chaumette, J. Catal. 168 (1997) 16.
[53] P. Arnoldy, J.A. Moulijn, J. Catal. 93 (1985) 38.
[54] A. Lapidus, A. Krylova, V. Kazanskii, V. Borovkov, A. Zaitsev, J. Rathousky, A. Zukal, M. Jancalkova, Appl. Catal. 73 (1991) 65.
[55] J. van de Loosdrecht, S. Barradas, E.A. Caricato, N.G. Ngwenya, P.S. Nkwanyana, M.A.S. Rawat, B.H. Sigwebela, P.J. van Berge, J.L. Visagie, Top. Catal. 26 (2003) 121.
[56] Y. Zhang, D. Wei, S. Hammache, J.G. Goodwin Jr., J. Catal. 188 (1999) 281.
[57] B. Jongsomjit, J. Panpranot, J.G. Goodwin Jr., J. Catal. 204 (2001) 98.
[58] B. Jongsomjit, C. Sakdamnuson, J.G. Goodwin Jr., P. Praserthdam, Catal. Lett. 94 (2004) 209.
[59] J.M. Jabłoński, J. Okal, D. Potoczna-Petru, L. Krajczyk, J. Catal. 220 (2003) 146.
[60] B. Jongsomjit, J.G. Goodwin Jr., Catal. Today 77 (2002) 191.
[61] A. Sirijaruphan, A. Horvath, J.G. Goodwin Jr., R. Oukaci, Catal. Lett. 91 (2003) 89.
[62] S. Storsæter, Ø. Borg, E.A. Blekkan, B. Tøtdal, A. Holmen, Catal. Today 100 (2005) 343.
[63] D. Schanke, A.-M. Hilmen, E. Bergene, K. Kinnari, E. Rytter, E. Ådnanes, A. Holmen, Catal. Lett. 34 (1995) 269.

[64] A.-M. Hilmen, O.A. Lindvåg, E. Bergene, D. Schanke, S. Eri, A. Holmen, Stud. Surf. Sci. Catal. 136 (2001) 295.
[65] J. Li, X. Zhan, Y. Zhang, G. Jacobs, T. Das, B.H. Davis, Appl. Catal. A 228 (2002) 203.
[66] J. Li, G. Jacobs, T. Das, Y. Zhang, B. Davis, Appl. Catal. A 236 (2002) 67.
[67] S. Krishnamoorthy, M. Tu, M.P. Ojeda, D. Pinna, E. Iglesia, J. Catal. 211 (2002) 422.
[68] G.W. Huber, C.G. Guymon, T.L. Conrad, B.C. Stephenson, C.H. Bartholomew, Stud. Surf. Sci. Catal. 139 (2001) 423.
[69] C.J. Bertole, C.A. Mims, G. Kiss, J. Catal. 210 (2002) 84.
[70] C.J. Kim, EP 339923 (1989).
[71] R.D. Jones, C.H. Bartholomew, Appl. Catal. 39 (1988) 77.
[72] E.P. Barrett, L.G. Joyner, P.P. Halenda, J. Am. Chem. Soc. 73 (1951) 373.
[73] J.L. Lemaitre, P.G. Menon, F. Delannay, in: F. Delannay (Ed.), The Measurement of Catalyst Dispersion, in: Characterization of Heterogeneous Catalysts, vol. 15, Dekker, New York, 1984, p. 299.
[74] Y. Li, Y. Fan, H. Yang, B. Xu, L. Feng, M. Yang, Y. Chen, Chem. Phys. Lett. 372 (2003) 160.
[75] G.L. Haller, D.E. Resasco, Adv. Catal. 36 (1989) 173.
[76] A. Kogelbauer, J.C. Weber, J.G. Goodwin Jr., Catal. Lett. 34 (1995) 259.
[77] Ø. Borg, M. Rønning, S. Storsæter, E.A. Blekkan, W. van Beek, A. Holmen, in preparation.
[78] C.J. Bertole, G. Kiss, C.A. Mims, J. Catal. 223 (2004) 309.
[79] Ø. Borg, S. Storsæter, E.A. Blekkan, S. Eri, E. Rytter, A. Holmen, in preparation.